Oxidation of Metals, Vol. 30, Nos. 3/4, 1988

Oxidation of High-Aluminum Austenitic Stainless Steels

Vijay Ramakrishnan,* James A. McGurty,* and N. Jayaraman*

Received December 22, 1987

The cyclical oxidation behavior of an austenitic stainless steel (24% Ni, 10% Cr, 5% Al, and balance Fe) has been evaluated in the temperature range 800–1300°C. The effects of trace elements such as S, Y, Zr, and Ti on the oxidation of the austenitic stainless steel have also been evaluated. The results indicate that Fe–Ni–Cr–Al stainless steels exhibit superior oxidation resistance up to 1300°C due to the formation of a very adherent and thin film of α-Al_2O_3.

KEY WORDS: austenitic steels; oxidation resistance; protective αAl_2O_3 film; kinetics.

INTRODUCTION

Since chromium is a strategically critical metal, it is important to consider ways to reduce the use of chromium in austenitic stainless steels. In this regard, McGurty and co-workers[1] have done significant alloy development work to replace chromium partially with aluminum in austenitic stainless steels. Several alloys with different compositions were examined for oxidation behavior, mechanical behavior, microstructure, welding properties and aqueous corrosion. Their important findings may be summarized as follows:

1. The high-Al, low-Cr stainless steels form a thin, adherent aluminum oxide film[2] during high-temperature oxidation, which is nonspalling and extraordinarily protective of the base metal.
2. These alloys contain only 10%Cr,[3] as compared with the 18–20% found normally in 300 series stainless steels (more than 40% savings on the strategically important Cr).

*Department of Materials Science and Engineering, University of Cincinnati, Cincinnati, Ohio 45221-0012.

0030-770X/88/1000-0185$06.00/0

3. The alloys containing 20% or more Ni are stable austenitic steels,[4] whereas the corresponding 300 series stainless steels are metastable, with reference to strain-induced martensitic transformation and sensitization in the temperature range of 450–800°C.
4. The high-Ni content in this alloy enables the steel to be a precipitation-hardenable alloy by formation of β-(Fe,Ni)Al[5] precipitates, which can be optimized to produce superalloy properties.
5. These alloys have good aqueous corrosion resistance[4] under nitric acid environments.
6. These alloys can be air induction melted. For example, 85 lb laboratory heats are routinely produced with better than 99% yield, and a yield of better than 97% is obtained for 1600 lb commercial heats.

This paper describes the oxidation of the Fe-24%Ni-10%Cr-5%Al alloy. The effects of varying the Y, Zr, Ti, and S contents on the oxidation behavior are also examined.

MATERIALS AND METHODS

Alloy Compositions

The chemical compositions of the alloys studied are shown in Table I. The alloy designated 880-4 is a stable austenitic alloy with 24.4%Ni, 9.73%Cr, 4.77%Al, and trace amounts of Zr(0.026%) and Y(0.094%); it is used here as a baseline alloy for oxidation studies. Alloy 880-5 has a chemistry similar to that of 880-4, except for its Y(0%) content. Alloys 896-1, -2, and -4 have slightly lower Ni(22.1%) and higher Zr(0.1%); they

Table I. Chemical Compositions of Alloys (wt.%)

Alloy	Ni	Cr	Al	Mn	Si	C	N	Zr	Y	Ca	S	Fe
880-4	24.4	9.73	4.77	0.14	0.41	0.027	0.021	0.026	0.094	0.003	—	Bal
880-5	25.4	9.95	4.90	0.14	0.12	0.023	0.010	0.034	0.000	0.004	21[a]	Bal
881-1	34.2	9.76	4.98	0.14	0.41	0.019	0.003	0.022	0.005	0.003	—	Bal
894-1	24.2	16.20	5.04	0.23	1.04	0.031	0.026	0.280	0.000	0.008	—	Bal
894-7	26.6	15.70	4.97	0.25	1.00	0.033	0.014	0.477	0.000	0.024	—	Bal
896-1	22.1	10.60	4.15	0.20	0.75	0.025	0.019	0.100	0.000	0.002	—	Bal
896-2	22.1	10.60	4.15	0.20	0.75	0.030	0.016	0.100	0.024	0.002	—	Bal
896-4	22.1	10.60	4.15	0.20	0.75	0.030	0.016	0.100	0.344	0.002	—	Bal
898-1	25.6	14.20	4.81	0.17	0.55	0.024	0.018	0.063	0.010	0.001	—	Bal
899-1	20.9	10.60	5.18	0.21	0.53	0.030	0.030	0.065	0.009	0.001	22[a]	Bal
14-1	22.0	10.00	5.10	0.03	169[a]	150[a]	—	23[a]	—	—	51[a]	Bal

[a]Denotes values in parts per million (ppm).

have progressively increasing Y contents (0, 0.024, and 0.344%, respectively) than does alloy 880-4. Alloy 898-1 has higher Cr(14.2%) than does 880-4. Alloy 899-1 has lower Ni(20.9%) and lower Y(0.009%). Alloy 881-1 has significantly higher Ni(34.2%) than does alloy 880-4. Alloys 894-4 and 894-7 have significantly higher Cr(16.2 and 15.7%, respectively) and higher Zr(0.280 and 0.477%, respectively) than does alloy 880-4. Finally, a relatively pure alloy, 14-1, was also examined. Extensive cyclic oxidation experiments over the temperature range of 800–1300°C were carried out on base alloy 880-4. On all the other alloys, cyclic-oxidation experiments were done only at an intermediate temperature of 1100°C. These experiments enabled us to evaluate not only the oxidation behavior over the temperature range but the effects of different alloying elements on the oxidation of this class of materials as well.

Oxidation Tests

Test coupons of dimensions 2.5 cm × 7.5 cm × 1.25 mm were used for the oxidation tests. The surfaces of these test coupons were mechanically polished to 600-grit finish and then ultrasonically cleaned. The specimen dimensions to within 0.02 mm and its weight to within 0.01 mg were measured before oxidation. Cyclic oxidation (between room temperature and the oxidation temperature) experiments were performed in air in resistance-heated tube furnaces kept at different oxidation temperatures in the range of 800–1300°C. The coupons were hung freely in the furnace using a thin alumina rod inserted through a small hole in each coupon. During each cycle, the coupons were exposed to the oxidation temperature for 20 hrs and cooled to room temperature. Weight-change measurements were made after each cycle. The experiments were done for 2500 hr at oxidation temperatures up to 1100°C. The higher-temperature tests were stopped at shorter times, depending on the extent of oxidation.

Metallography, Scanning Electron Microscopy, and X-Ray Diffraction

The oxidized specimens were subjected to optical metallography and X-ray diffraction (XRD). Small sections of the specimens were prepared by standard metallographic procedures for optical microstructural examination of the cross section and the oxide-metal interface. Scanning electron microscopy (SEM) was performed on the samples using a Cambridge 600 Stereoscan fitted with an energy-dispersive X-ray analyzer (EDAX). Another part of the oxidized specimens was subjected to qualitative phase analysis by XRD. A Philips-Norelco powder diffractometer with a graphite-crystal, diffracted-beam monochromator was used. CuK_{α} radiation with the X-ray tube operating conditions of 40 kV and 20 mA was used.

RESULTS

Weight-Change Measurements

Figure 1 plots the weight change of the oxidized samples vs the number of oxidation cycles at temperature. These plots show that alloy 880-4 has very little weight change, even at 1300°C. Parabolic rate constants were determined from these weight-change measurements, which were subsequently used for determining an apparent activation energy for the process of oxidation. Figure 2 shows the photographs of the six 880-4 samples at the completion of the cyclic oxidation tests. For the sake of comparison, samples of 80Ni-20Cr (Nichrome V) alloy oxidized under similar conditions are included. The alloy 880-4 showed much superior oxidation resistance as compared with the 80Ni-20Cr alloy.

Figure 3 shows the effect of alloying elements on the oxidation behavior of the Fe-Ni-Cr-Al alloy. The effect of yttrium addition on oxidation resistance is shown in Fig. 3a, which compares the weight-change characteristics of the 896-1(0% Y), 896-2 (0.024% Y), 880-4 (0.094% Y), and 896-4

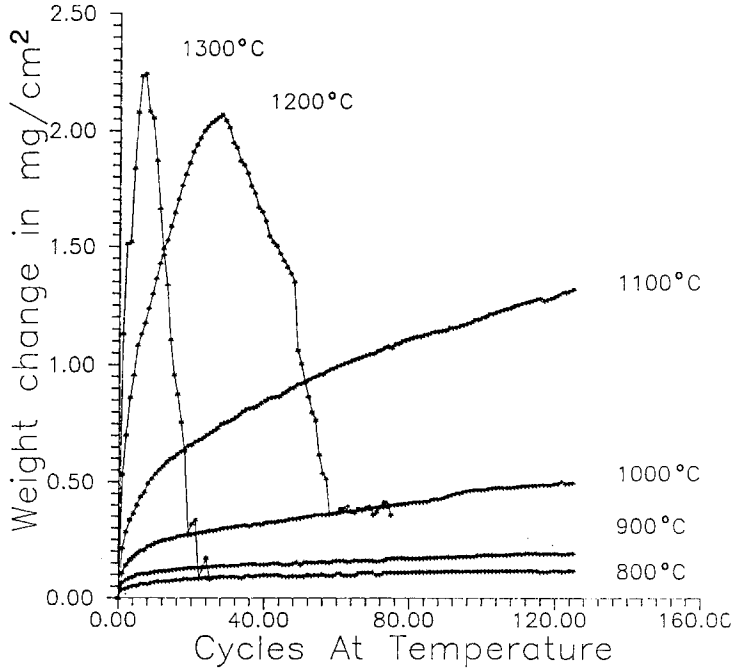

Fig. 1. Weight-change data for the samples of alloy 880-4 plotted against the number of oxidation cycles at temperature.

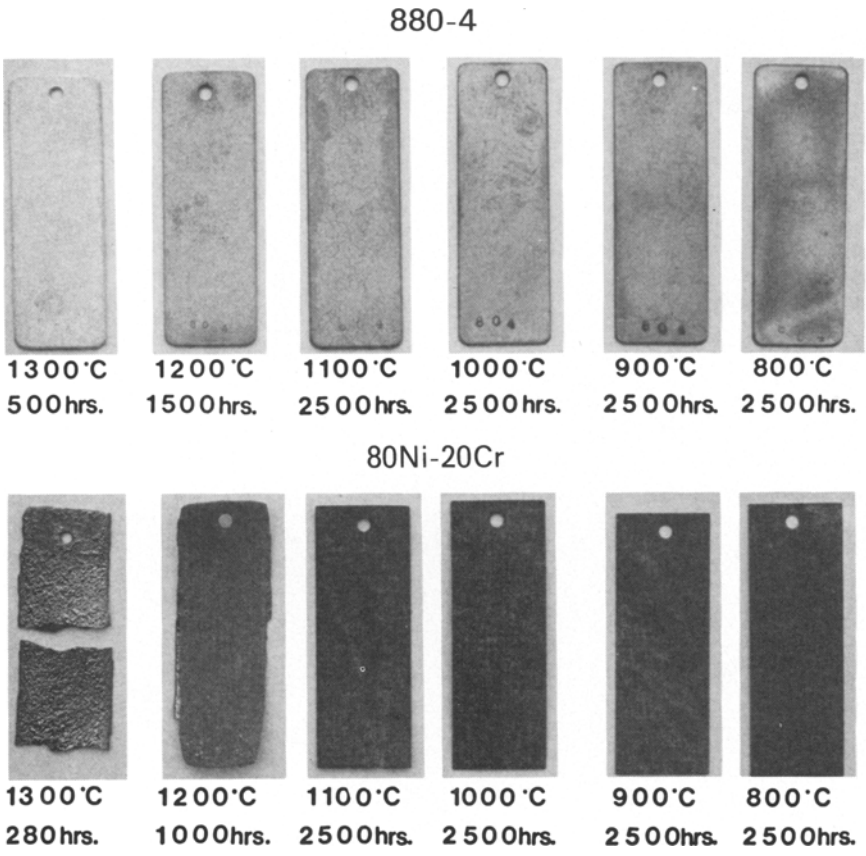

Fig. 2. Appearance of the alloys 880-4 and 80 Ni-20 Cr alloys after cyclical oxidation at the temperature indicated for the indicated period of time.

(0.344% Y) alloys. These data show that the addition of yttrium in amounts greater than 0.1% increases the rate of oxidation. Figure 3b compares the oxidation resistance of the 880-4 (0.026% Zr), 894-4 (0.280% Zr), and the 894-7 (0.477% Zr) alloys, to study the effects of zirconium on the oxidation resistance of these alloys. As shown, increasing the amount of zirconium increases the rate of oxidation of these alloys. Figure 3c compares the weight-gain characteristics of the 881-1 (0% Ti) and the 881-8 (1% Ti) alloys to obtain the effects of titanium on these alloys. The presence of 1% titanium in the 881-8 alloy substantially increases the oxidation rate of the alloy. The data shown in Fig. 3d compare the weight-change characteristics of the 14-1 (51 ppm S), 899 (22 ppm S), and 880-5 (21 ppm S) alloys to study the effect of sulfur content on the oxidation resistance of these alloys. Figure

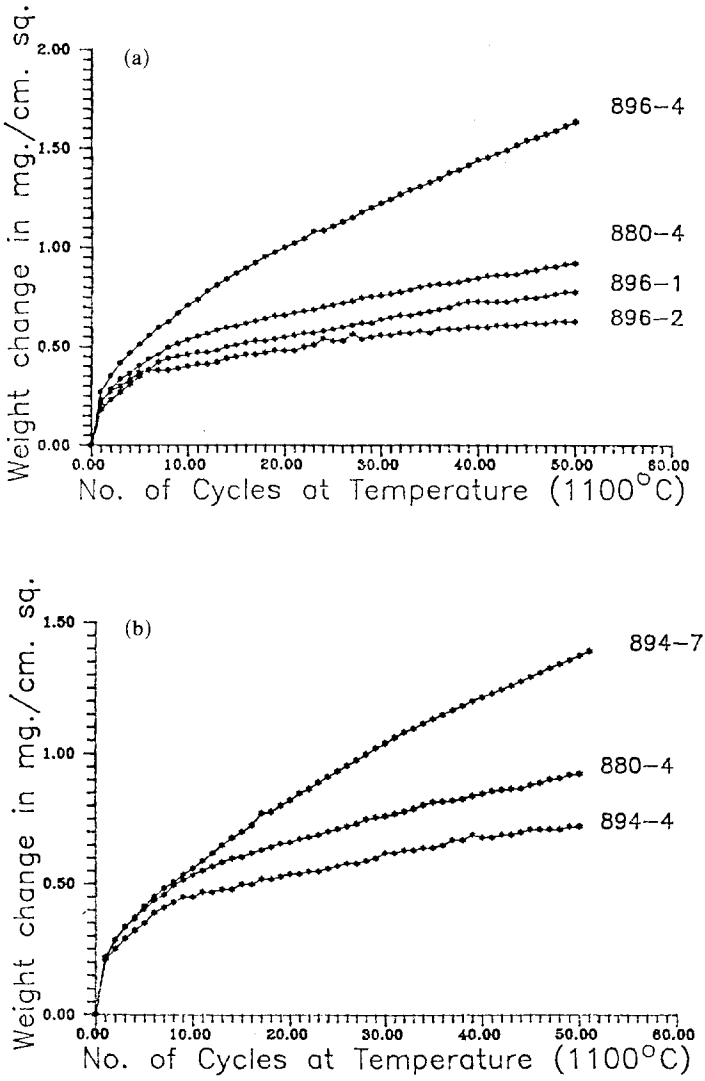

Fig. 3. Comparisons of weight-gain data. (a) To obtain the effect of Y on oxidation resistance by 896-1 (0% Y), 896-2 (0.024% Y), 880-4 (0.094% Y), and 896-4 (0.344% Y). (b) To obtain the effect of Zr on oxidation resistance 894-7 (0.477% Zr), 880-4 (0.026% Zr) and 894-4 (0.280% Zr) alloys. (c) To obtain the effect of Ti on oxidation resistance by 881-1 (0% Ti) and the 881-8 (1% Ti). (d) To obtain the effect of S on oxidation resistance by 14-1 (51 ppm S), 899 (22 ppm S) and 880-5 (21 ppm S).

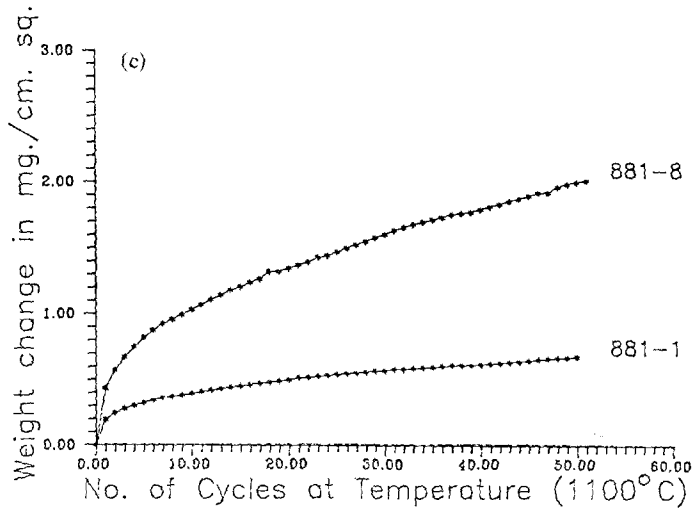

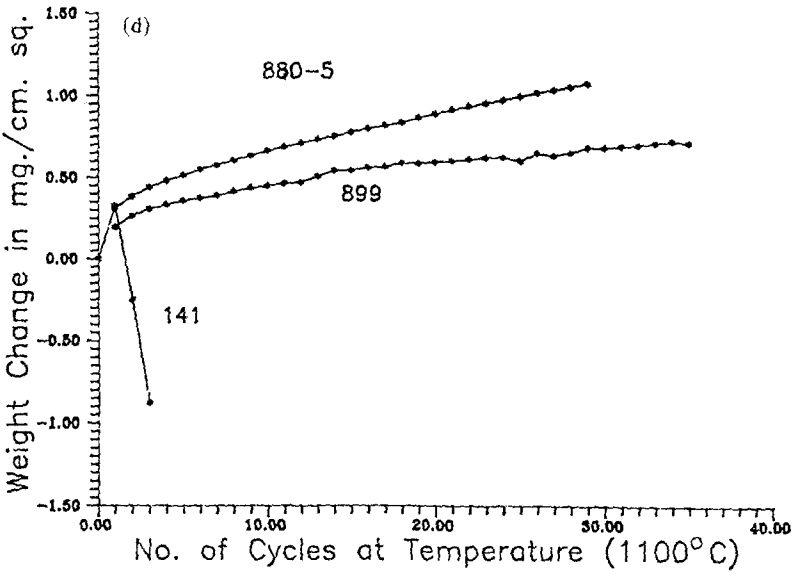

Fig. 3. Continued.

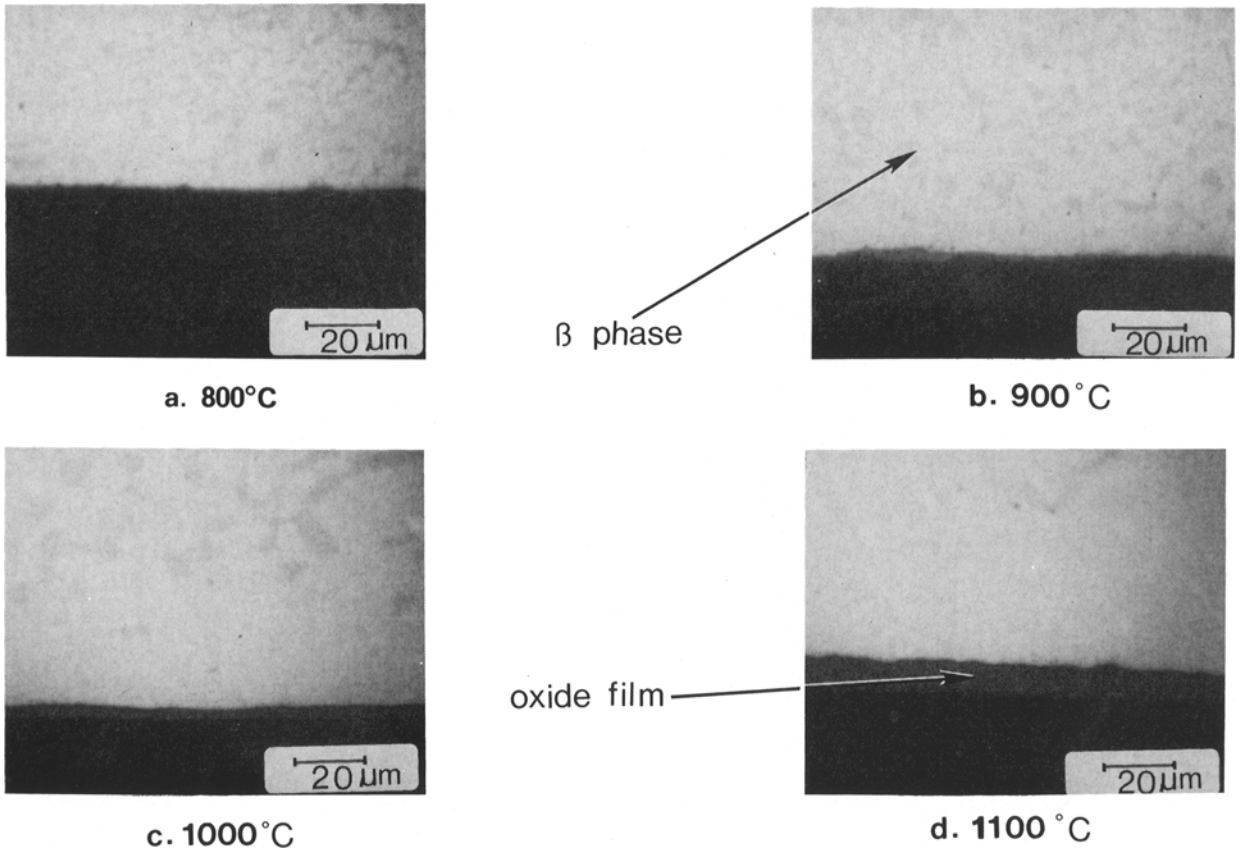

Fig. 4. Microstructure at the oxide film–metal interface of alloy 880-4. (a) Oxidized for 2500 hr at the temperatures indicated showing the precipitate β-phase and the uniform oxide film produced up to 1100°C. (b) Oxidized for 2500 hr at 1000 and 1100°C for 2500 hr, at 1200°C for 1500 hr and at 1300°C for 500 hr, showing the β-depleted zone at lower temperatures and the irregular oxide film at higher temperatures.

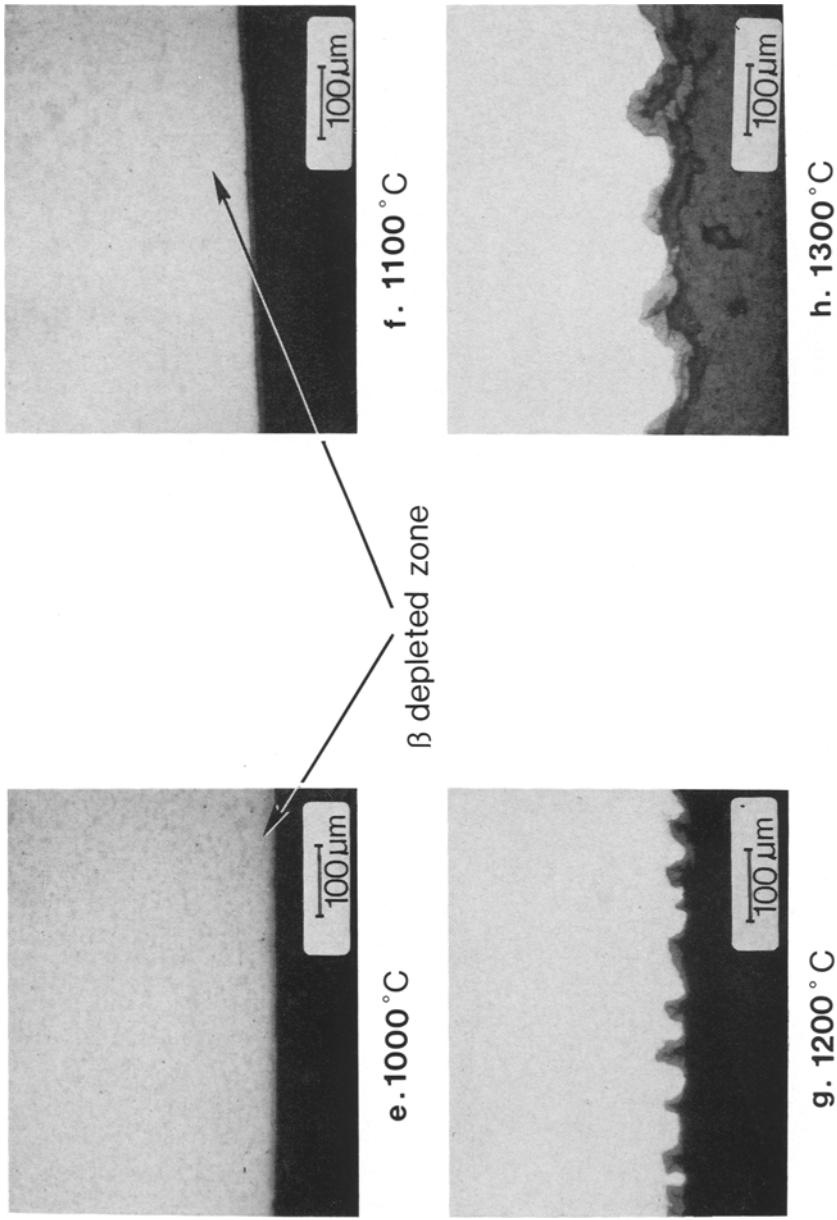

Fig. 4. Continued.

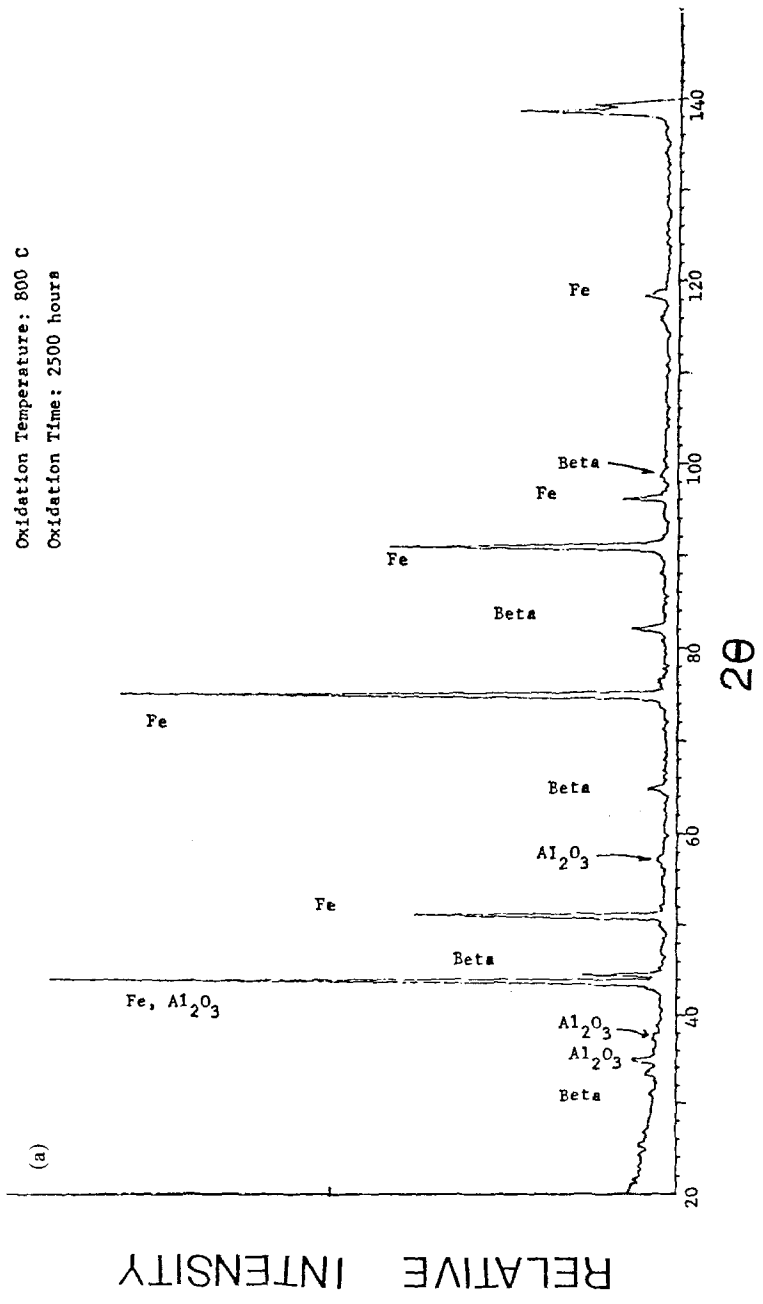

Fig. 5. Full X-ray scans. (a) Sample oxidized at 800°C, showing peaks of Fe, β-phase, and Al_2O_3. (b) Sample oxidized at 1100°C, showing peaks of Fe and Al_2O_3. (c) Sample oxidized at 1300°C, showing peaks of Al_2O_3 and Fe.

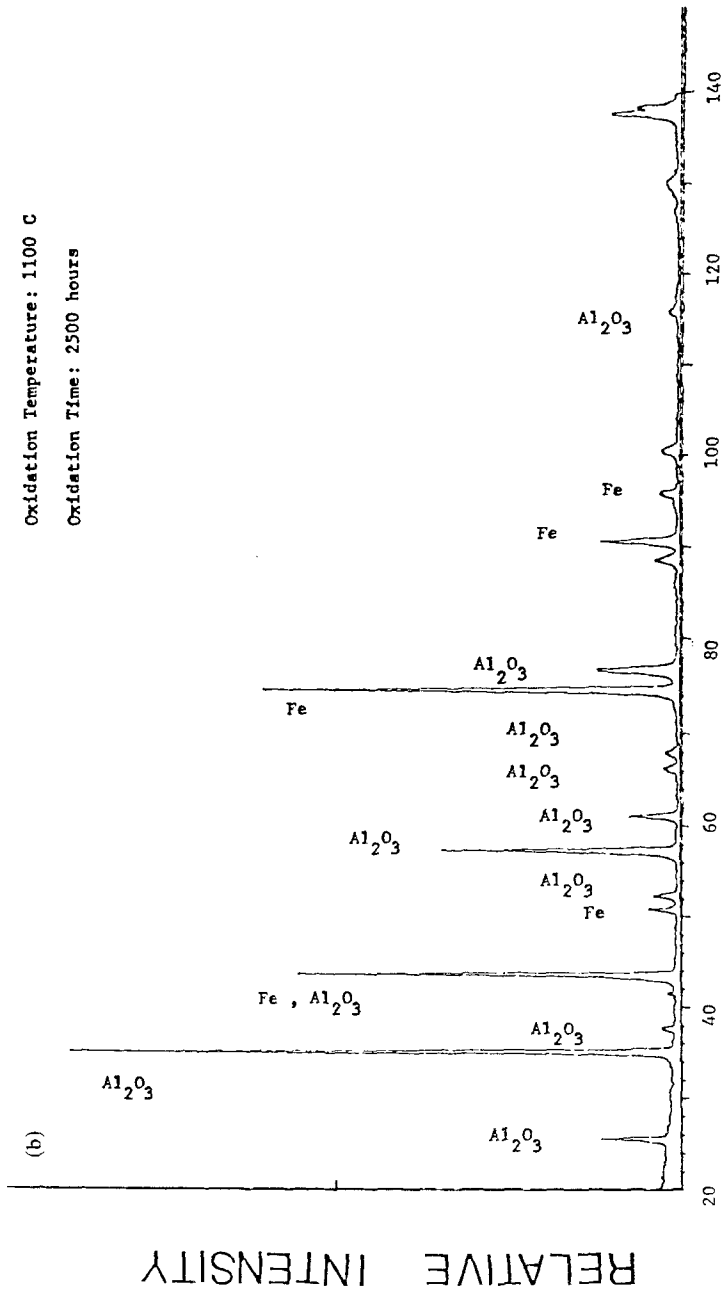

Fig. 5. Continued.

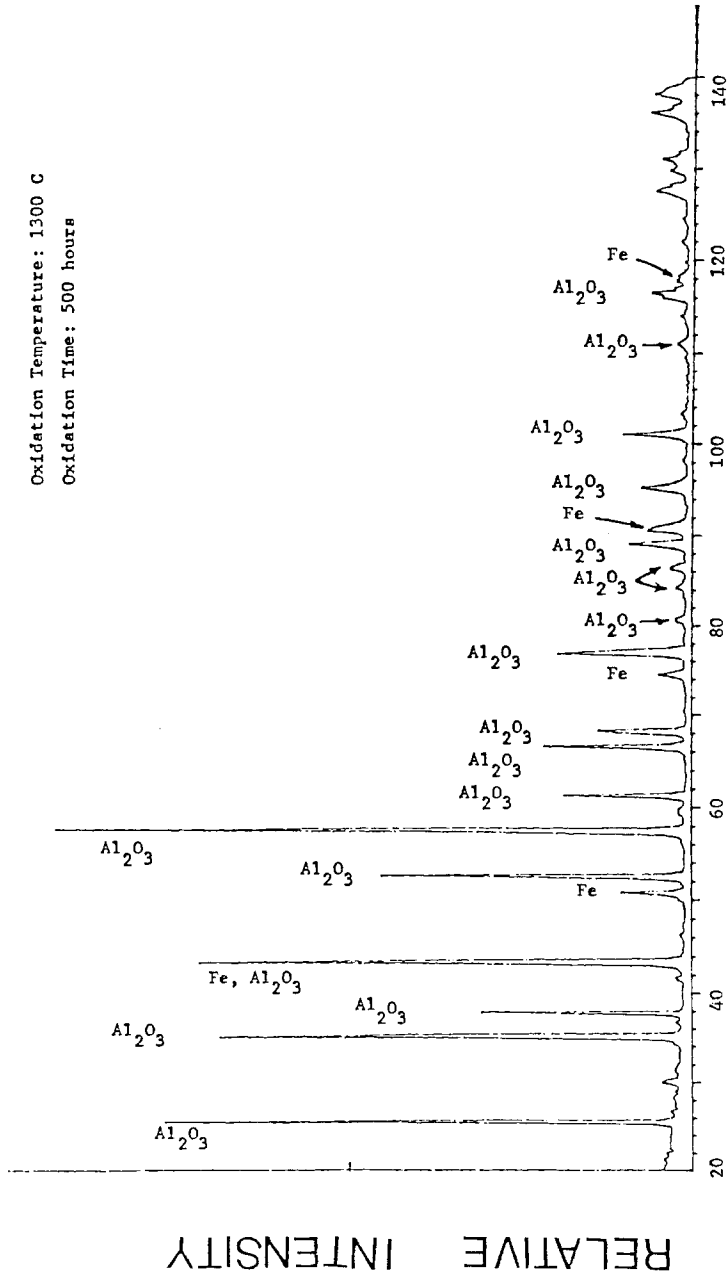

Fig. 5. Continued.

3c demonstrates that sulfur has a catastrophic effect on the oxidation resistance as shown by the catastrophic spalling of the oxide film that forms on the 14-1 high-sulfur-content alloy.

Metallographic Evaluations

Figure 4a–h shows optical micrographs of the specimens of alloy 880-4 oxidized in the range 800–1300°C. In general, the oxide-metal interface is straight in the temperature range 800–1100°C (Fig. 4a–d) and very irregular at higher temperatures (Fig. 4e, h). Large β-phase precipitates [(Fe,Ni)Al] can be seen in these micrographs, as these precipitates tend to overage even at lower temperatures. The β-depletion zone, which is an indication of depletion of Al near the oxide-metal interface can be seen in these micrographs to increase in size with increasing oxidation temperature. The oxide scale, the β-depletion zone, and the β-phase precipitates are indicated on the micrographs.

Precise oxide-scale thickness and depletion-zone widths were determined using SEM. The data were then used to determine the apparent activation energy for the process of oxidation and depletion of Al in the metal.

X-Ray Diffraction

Complete XRD scans for typical 880-4 samples oxidized at temperatures 800, 1100, and 1300°C are shown in Fig. 5a–c. Phases such as Fe(γ), α-Al_2O_3, and β-(Ni-Al) were identified in these X-ray scans. α-Al_2O_3 is the only oxide phase detected on the surface, and the relative amount of αAl_2O_3 increases with increasing oxidation temperature.

DISCUSSION

Oxidation of Fe–24.5Ni–9.73Cr–5Al Alloy

The weight-gain data obtained for the 880-4 alloy for oxidation in the temperature range 800–1100°C were analyzed using regression analysis and determined to be parabolic. The parabolic rate constant, K_p was found to increase with increasing oxidation temperature from about 10^{-15} g^2-cm^4/sec at 800°C to 10^{-11} g^2-cm^4/sec at 1300°C.

Hindam and Whittle[6] compiled data on the growth kinetics of Al_2O_3 on several Al-containing alloys. Figure 6 compares the K_p values for the alloy 880-4 with other aluminum-containing alloys described by Hindam and Whittle. It can be seen that the alloy 880-4 has a considerably lower

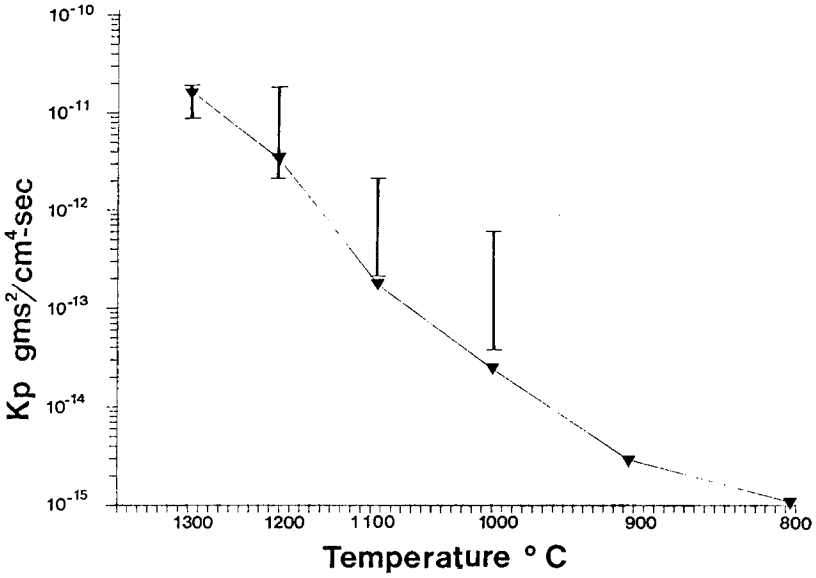

Fig. 6. K_p values for alloy 880-4 compared with alloys described by Hindam and Whittle.[6] K_p values for alloys from the latter lie on the band indicated; those for alloy 880-4 are indicated by the triangle.

parabolic rate constant compared with that of all the alloys reported by these investigations over the entire range. This is particularly impressive considering the fact that the alloys showing superior oxidation resistance in Fig. 6 are noble metal-based alloys. Using the weight-gain data for alloy 880-4, an apparent activation energy oxidation in the temperature range 800–1100°C was determined to be 65 kcal/mole.

Using the oxide-film thickness and the β-depletion-zone widths determined from SEM analysis, the effective diffusion coefficients (D_{eff}) for the oxidation and Al-depletion processes were determined using the following equation suggested by Hindam and Whittle[6]:

$$x^2 = D_{\text{eff}} * t$$

where x is the oxide-scale thickness (or depletion-zone width) at the given temperature, t is the oxidation time in seconds, and D_{eff} is the effective diffusion coefficient for the oxide-film growth process or the Al-depletion process.

Apparent activation energies for the above two processes were determined by fitting the data to Arrhenius rate equations. All of these data are listed in Table II. The data presented in the table are restricted to the

Table II. K_p and D_{eff} Values Calculated from Weight Gain, Oxide-Scale Thickness, and Al-Depletion-Zone Size Measurements.[a]

Temperature (°C)	K_p (from weight-gain data) (g^2-cm^4/sec)	D_{eff} (from Al_2O_3 thickness) (cm^2/sec)	D_{eff} (from Al-depletion zone) (cm^2/sec)
900	3.0×10^{-15}	1.2×10^{-15}	1.8×10^{-15}
1000	2.4×10^{-14}	1.4×10^{-14}	4.4×10^{-13}
1100	1.7×10^{-13}	8.4×10^{-14}	1.0×10^{-11}
Pre-exponential factor, A	3.8×10^{-3}	6.5×10^{-3}	1.6×10^{11}
Apparent Q, kcal/mole	65	68	138

[a]The apparent activation energy Q values were determined by fitting the K_p and D_{eff} data to an Arrhenius-type relationship; in all instances, the fitting was excellent, yielding a correlation coefficient of better than 99.9%. The pre-exponential factors A have the same units as K_p and D_{eff}.

temperature range 900–1100°C since precise measurement of the oxide scale thickness and of the depletion zone width was not possible at other temperatures. At 800°C, the oxide scale and the depletion zone were too small to detect; at 1200 and 1300°C, the oxide-metal interface was irregular and therefore introduced a large error in measurement.

We can see from Table II that the apparent activation energy for the weight-gain data and for the oxide-scale-growth data are almost the same, while the aluminum depletion process has a higher apparent activation energy. Unfortunately, no reliable diffusion data are available for Al or oxygen diffusion in Al_2O_3 or Al diffusion in γ-iron at the temperature ranges of this study. Therefore, any mechanism proposed for the oxidation process based on the above observations can at best be speculative in nature. The relatively high apparent activation energy and pre-exponential factor for the Al-depletion process may be attributed to the fact that the process of Al depletion involves resolution of the β-(Fe,Ni)Al precipitates and subsequent diffusion of Al to the oxide-metal interface. It should be noted that the β-precipitates are otherwise stable at these temperatures.

Because the α-Al_2O_3 oxide film is very adherent and the oxidation rate very small, the growth of the oxide film appears to be controlled by the outward diffusion of Al cations. This would imply that the freshly forming oxide would form at the oxide-air interface, as opposed to the metal-oxide interface by the inward diffusion of oxygen anions. The formation of the new oxide layer at the oxide-air interface, which is a free surface would explain the extraordinary adherence of the oxide film to the base metal and the absence of any breaks in the oxide film-metal interface despite the large volume change associated with the formation of Al_2O_3 from Al.

Effect of Alloying Elements on Oxidation Rate

The effects of various alloying elements on the oxidation behavior of the Fe-Ni-Cr-Al alloy are consistent with observations made by previous researchers. For example, Mrowec and Werber[7] observed that small additions of yttrium improved oxidation resistance in Cr steels. Observations from the present study on the alloys 896-1 and 896-2 are consistent with this finding. Tien and Pettit[8] observed that larger additions of Y increased the oxidation rate of Cr steels. Again, in comparison with alloys 896-1 and 896-2, alloys 880-4 and 896-4 showed higher oxidation rates. Truman and Pirt[9] observed that the addition of Ti increased the oxidation rate of Cr steels, which is consistent with observations in this study in alloys 881-1 and 881-8 (1% Ti). Kahn *et al.*[10] observed that the addition of Zr generally increased the oxidation rate, which is consistent with the present observations in alloys 894-4 and 894-7. The effect of increasing S from 21 to 51 ppm seemed to affect the oxidation very drastically and the mechanism proposed by Mrowec and Werber[11], that of formation of low-melting, sulfide-oxide eutectics, could offer an explanation for this effect.

CONCLUSIONS

Fe-24Ni-10Cr-5Al alloy shows excellent oxidation resistance up to 1100°C and is moderately oxidation resistant up to 1300°C. The excellent oxidation resistance is attributed to the formation of a nonspalling αAl_2O_3 oxide film. There was no internal oxidation up to 1300°C. The addition of alloying elements, such as zirconium, yttrium, titanium, and sulfur, generally increased the oxidation rate. However, when added in small quantities (up to 0.02%), yttrium has a beneficial effect.

REFERENCES

1. J. A. McGurty, U.S. Pat. No. 4,086,085. (1978).
2. J. A. McGurty, R. Nekkanti, E. Rosa, and J. Moteff, in *Alternative Alloying for Environmental Resistance* (The Metallurgical Society, 1987), p. 249.
3. J. A. McGurty, R. Nekkanti, E. Rosa, and J. Moteff, in *High Temperature Alloys: Theory and Design*, J. O. Stiegler, eds. (TMS-AIME Publication, 1984), p. 473.
4. J. A. McGurty, R. Nekkanti, D. Cornish, and J. Moteff, in *Alternative Alloying for Environmental Resistance* (The Metallurgical Society, 1987), p. 407.
5. J. A. McGurty, R. Nekkanti, and J. Moteff, *J. Met.* **37**, 22 (1986).
6. H. Hindam and D. P. Whittle, *Oxid. Met.* **18**(5/6), 245 (1982).
7. S. Mrowec and T. Werber, *Gas Corrosion of Metals* (National Bureau of Standards and the National Science Foundation, Washington, D.C., 1978), p. 349.
8. J. K. Tien and F. S. Pettit, *Metall. Trans.* **3**, 1587 (1972).
9. J. E. Truman and K. R. Pirt, *Br. Corros. J.* **13** (1978).
10. A. S. Kahn, C. E. Lowell, and C. A. Barrett, *J. Electrochem. Soc.* **127**, 671 (1980).
11. S. Mrowec and T. Werber, *Gas Corrosion of Metals* (National Bureau of Standards and the National Science Foundation, Washington, D.C., 1978), p. 350.